Risk-bounded and Fairness-aware Path Planning for Urban Air Mobility Operations under Uncertainty

Pengcheng Wu^a, Junfei Xie^b, Yanchao Liu^c, Jun Chen^{d,*}

Department of Aerospace Engineering, San Diego State University, 5500 Campanile Drive, San Diego, CA, 92182, U.S.A.

Abstract

Collision avoidance is an important issue in the field of the autonomous operations of aerial vehicles in dynamic and uncertain urban environments. This paper introduces a risk-bounded and fairness-aware path planning algorithm for multiple electrical vertical take-off and landing (eVTOL) aircraft operating in such environments. This algorithm advances the sampling-based path planning with the risk domain formulation to generate stochastically safety assured collision-free paths that are robust to both vehicle and environmental obstacle uncertainties for multiple eVTOL aircraft. To address the concern of flight fairness between different eVTOLs in the free flight airspace, the strategy of permit assignment is introduced. By incorporating the risk domain formulation into the sampling-based path planning with the strategy of permit assignment, the algorithm proposed in this paper not only inherits the computational advantage of the sampling-based methods, but also guarantees a stochastically feasible flying zone at every time step. Simulation studies demonstrate the promising performance of the proposed algorithm.

Keywords: Urban Air Mobility, eVTOL, Risk Domain, Fairness-awareness, Risk-bounded Path Planning

1. INTRODUCTION

1.1. Motivations

Urban air mobility (UAM) envisions a safe and efficient air transportation system that employs autonomous aircraft operating at lower altitudes within urban and suburban areas. Enabled by the technological advancements in automation, electrification, and vertical

^aDepartment of Mechanical and Aerospace Engineering, University of California San Diego, 9500 Gilman Drive, La Jolla, CA, 92093, U.S.A.

^bDepartment of Electrical and Computer Engineering, San Diego State University, 5500 Campanile Drive, San Diego, CA, 92182, U.S.A.

^cDepartment of Industrial and Systems Engineering, Wayne State University, 4815 4th Street, Detroit, MI 48201, USA

^dDepartment of Aerospace Engineering, San Diego State University, 5500 Campanile Drive, San Diego, CA, 92182, U.S.A.

^{*}Corresponding author

Email addresses: pcwupat@ucsd.edu (Pengcheng Wu), jxie4@sdsu.edu (Junfei Xie), yanchaoliu@wayne.edu (Yanchao Liu), jun.chen@sdsu.edu (Jun Chen)

take-off and landing, autonomous applications using electrical vertical take-off and landing (eVTOL) aircraft in UAM, such as passenger mobility [1], goods delivery [2], and drone-assisted urban logistics [3], are drawing increasing attention in recent years. Compared with traditional fixed-wing aircraft or helicopters, eVTOL aircraft combine the advantages of high-speed cruising and flexible maneuvering. At present, most studies of UAM concentrate on the structured airspace where corridors are specified and eVTOL aircraft need to follow the fixed routes inside the corridors for conservative safety assurance. In contrast, the notion of the free flight airspace was presented for future air transportation and it is capable of utilizing more airspace volume than the structured airspace. Despite the great benefits, the development of free flight still faces great challenges, among which flying safety and flight fairness are two of the most critical concerns for the successful operations of a team of eVTOLs in UAM.

For flying safety and reliability, the requirement of collision avoidance should be fulfilled in path planning for eVTOLs [4, 5]. In a free flight framework, every aircraft is responsible for its own safety assurance. Without the protection of structured airways, eVTOLs need to rely on the collision avoidance system to detect and avoid conflicts. However, the presence of various forms of uncertainties in real scenarios may cause the failure of eVTOL operations based on the current collision avoidance systems. Ideally, we expect to find trajectories for a team of eVTOLs so that no collision will occur if all the eVTOLs in the team follow the found trajectories. This is infeasible because of the presence of location uncertainty. Alternatively, we propose to generate trajectories which guarantee the probability of loss of sufficient separation is bounded by a risk level if eVTOLs follow the generated trajectories. Flight fairness among different aircraft is another important concern when it comes to free flight in UAM [6]. Without considering flight fairness, the running of the developed path planning algorithm may lead to the delay of certain eVTOLs in the system, which does not make sense in real scenarios. Instead, strategies like adjusting the flight priority can be designed to help improve the flight fairness between different eVTOLs.

To address the aforementioned issues, it is critical to find a proper balance between path planning safety/fairness and efficiency. In this paper, we develop a risk-bounded and fairness-aware path planning algorithm based on a sampling-based method that generates probabilistically guaranteed collision-free paths for a team of eVTOLs under different forms of uncertainty.

1.2. Related Work

The location uncertainty is an important concern when it comes to planning the collision-free path for a team of eVTOLs. Two different forms of uncertainty are usually found in path planning scenarios involving collision avoidance [7, 8]. One is vehicle uncertainty, which arises from factors such as the inaccurate measurement of self-position or disturbance of wind, and is associated with every eVTOL in the team; the other one is obstacle uncertainty, which is caused by the inaccuracy of eVTOLs' onboard sensors, and is associated with every obstacle to be evaded by all the eVTOLs. To address vehicle uncertainty, Prentice et al. considered a linear system subject to Gaussian process noise to achieve the desired probability of feasibility [9]. Pepy et al. sought guaranteed feasibility for a nonlinear system subject to bounded state uncertainty of the vehicle [10]. In addition to the vehicle uncertainty, many existing works have also focused on the obstacle uncertainty. Luders et al. studied probabilistic

robustness to both process noise and uncertain dynamic obstacles following deterministic trajectories [11]. However, these works treated vehicle uncertainty and obstacle uncertainty separately, which made design and analyses complicated. In this paper, we introduce the transformation of relative uncertainty, which reduces different forms of uncertainty into a common one. This provides a unified and efficient way to address different forms of uncertainties.

For a single eVTOL operating in a complex and dynamic environment, one effective way to achieve a balance between the planning conservatism and efficiency is through formulating the probabilistic bound for collision with obstacles as the chance constraints, meaning that the probability of constraint violation does not exceed a prescribed threshold [12, 13]. This can be achieved by converting probabilistic constraints into equivalent deterministic ones through a transformation. In previous studies, Blackmore et al. proposed a chance constraints formulation for a system subject to Gaussian noise, by assuming that all environmental obstacles have static and deterministic locations [14, 15]. Toit et al. developed a chance constrained framework that considered other types of uncertainties [16]. Luders et al. extended the chance constraints formulation to allow for dynamic and probabilistic obstacles [11]. Manuel et al. restricted each polyhedral obstacle to be a cuboid and then obtained a tight quadratic bound for collision avoidance analytically [17]. In contrast to these studies, we propose a different risk domain formulation in this paper. Compared to existing methods which established an approximate convex polygon and then found the distance between a point and a straight line, our method is an ellipse that has an explicit mathematical expression and we figure out an exact solution to the distance between a point and an ellipse. Also, we take into consideration the safety ranges of the eVOTL aircraft.

The path planning of multiple eVTOLs in a complex and dynamic environment has also been investigated [7]. A team of eVTOLs can accomplish multiple tasks in parallel and perform far more complicated tasks than a single eVTOL operating alone. Compared with a single eVTOL, the path planning for a team of eVTOLs needs to consider not only the collisions with environmental obstacles but also the collisions between different eVTOLs [18]. To address this challenge, Scerri et al. proposed a deconfliction strategy in which the team must reach a consensus on path feasibility for any updated path [19]. Another remarkable approach was proposed by Purwin et al., in which vehicles reserve regions of the map to move in and must reach a consensus on any modifications to these regions [20]. Reachability-based planning approaches have also been studied for collision avoidance along intersecting paths [21, 22]. Desaraju et al. proposed an algorithm for multi-aircraft systems with complex constraints [23]. However, in the aforementioned studies, either the aircraft in the team or environmental obstacles are assumed to be deterministic, which is a strong assumption in realistic operations. In this paper, we propose a path planning algorithm for a team of eVTOLs operating in complex and dynamic environments under uncertainties. For the conflict detection and avoidance of a team of multiple eVTOLs, the risk domain formulation of the conflict between one pair of eVTOLs in the team is first considered. Then that formulation is applied to every pair of eVTOLs in the team, so that we can ultimately perform inter-agent conflict checking between any two eVTOLs in the team. In addition, the priority between flights is a major issue when it comes to the air traffic management (ATM). For the free flight in UAM, this issue hasn't been fully investigated yet [6]. In this

paper, we present a strategy to address the concern of flight fairness, especially in the free flight airspace of UAM.

There are various methods which contribute to solving such a path planning problem, like mixed-integer linear programming (MILP) [24], nonlinear programming [25], mixed-integer quadratic programming [26], second-order cone programming [27]. However, the intensified computational load will lead to the intractability of those aforementioned computational methods when the dimensions of the space grow. Different from those computationally intensive optimization approaches which scale poorly with the number of constraints imposed by the complex environment, the sampling-based methods can efficiently model complex dynamics and constraints and scale well [28]. The rapidly-exploring random tree (RRT) [29, 30] and Monte Carlo tree search (MCTS) [6] are two state-of-the-art representatives of the sampling-based methods, which grow trees to search the configuration space and perform trajectory-wise collision checking. However, the traditional sampling-based methods didn't consider the probabilistic constraints within their formulations, leading to the consequence that they cannot be used to directly deal with obstacles whose locations are uncertain. Also, the existing methods have been rarely used to solve problems involving the flight fairness between different flights in a system consisting of multiple eVTOLs [6]. To break through this limitation, we incorporate the risk domain formulation into the development of the proposed path planning algorithm based on the essentials of the sampling-based method of tree search, and address the flight fairness concern using the strategy of permit assignment. The resulting method not only inherits the computational advantage of the traditional sampling-based methods, but also guarantees probabilistic feasibility for the planned path at every time step.

1.3. Contributions and Structure

In this paper, we come up with a risk-bounded and fairness-aware path planning algorithm based on sampling-based method of tree search for the guidance of a team of eVTOLs in the free flight airspace of UAM. The major contributions of this paper are summarized as follows:

- 1. An efficient risk domain formulation is presented to deal with location uncertainty. It transforms the original stochastic uncertainty into deterministic ones, which greatly saves computational time while guaranteeing collision avoidance with high probability. The formulated risk domain has an explicit mathematical expression, and also takes the safety ranges of all the eVTOLs and obstacles into consideration.
- 2. The method of relative uncertainty transformation is introduced and implemented within the free flight airspace of UAM, and thus different forms of uncertainties can be transformed into a common one. This provides a unified and efficient way to deal with different forms of uncertainties.
- 3. The strategy of permit assignment is proposed to solve the path planning problem involving flight fairness between different eVTOLs in a system consisting of multiple aircraft. This helps achieve a trade-off between planning efficiency and flight fairness in the free flight airspace of UAM.

4. The risk-bounded and fairness-aware path planning algorithm based on the sampling-based method of tree search is developed for a team consisting of multiple eVTOLs. It is integrated with the risk domain formulation to provide safety assured and feasible trajectories for all the eVTOLs in the team. The strategy of permit assignment is also combined with the algorithm to address the concern of flight fairness in path planning for UAM.

The remaining part of this article is organized as follows. In Section 2, the problem statement is presented. In Section 3, the efficient risk domain formulation is proposed and fully discussed. In Section 4, the proposed risk domain formulation is incorporated into the development of the sampling-based path planning algorithm for eVTOLs, combined with the strategy of permit assignment to ensure flying safety and flight fairness. In section 5, the feasibility of the proposed algorithm is verified through simulation studies. Finally, we conclude this article in Section 6.

2. PROBLEM STATEMENT

For an aerial vehicle, its location x_t at a particular time t may be stochastic, due to vehicle uncertainty arising from factors like the inaccurate measurement of self-position or the disturbance of wind. Especially, under the assumption of Gaussian distribution, the location x_t obeys

$$\boldsymbol{x}_t \sim \mathcal{N}(\boldsymbol{\mu}_{t*}, \boldsymbol{\Sigma}_*)$$
 (1)

where $\mathcal{N}(\boldsymbol{\mu}_{t*}, \boldsymbol{\Sigma}_*)$ represents a Gaussian distribution with a time-varying mean $\boldsymbol{\mu}_{t*}$ and a time-invariant covariance $\boldsymbol{\Sigma}_*$.

To operate safely in a dynamic uncertain environment, each eVTOL should seek to avoid collisions with other eVTOLs and environmental obstacles in the system. This can be achieved by introducing the following constraints

$$\mathbf{x}_t \notin \mathcal{X}_t, \quad \forall t$$
where $\mathcal{X}_t := \left(\bigcup_{i=1}^{N-1} \mathcal{X}_{ti}\right)$ (2)

In the above constraints, we use \mathcal{X}_{ti} to denote the area in which obstacle/eVTOL i may be located at time t due to location uncertainty, where $i \in \{1, 2, ..., N-1\}$ and N is the total number of all the eVTOLs and environmental obstacles involved. Thus, from the perspective of the current aircraft, the remaining N-1 aircraft and environmental obstacles are viewed as obstacles to evade. \mathcal{X}_t is formed by all the other eVTOLs and environmental obstacles that the current eVTOL seeks to avoid. We call such an area the possible region. Note that, from the perspective of the current eVTOL, all the other eVTOLs in the system actually can be viewed as dynamic obstacles to avoid. The time dependence of \mathcal{X}_t allows the inclusion of either static or dynamic obstacles. For the current eVTOL in the system, all the other eVTOLs need to be treated as dynamic ones. In what follows, if not specified, when it comes to obstacles, we always refer to both environmental obstacles and the other eVTOLs except the current eVTOL.

From the perspective of the current eVTOL, the possible region \mathcal{X}_{ti} formed by an obstacle i at time step t is modeled by the following equation, assuming the location \mathbf{c}_{ti} of the obstacle i obeys Gaussian distribution,

$$\mathcal{X}_{ti} = \{ \boldsymbol{x} \in \mathbb{R}^d \mid ||\boldsymbol{x} - \boldsymbol{c}_{ti}|| \le r_i \}, \quad \forall t, i.$$

$$\boldsymbol{c}_{ti} \sim \mathcal{N}(\boldsymbol{\mu}_{ti}, \boldsymbol{\Sigma}_i)$$
(3)

where r_i is the safety range for the current eVTOL to stay away from the *i*th obstacle to ensure safety, which depends on the speed of the obstacle [31]. For simplicity, r_i is assumed to be a constant for every obstacle *i* and it may vary across different obstacles. In addition, c_{ti} represents the position of the *i*th obstacle at time *t*, which is an independent Gaussian random variable, i.e., $c_{ti} \sim \mathcal{N}(\mu_{ti}, \Sigma_i)$ with a time-varying mean μ_{ti} and a time-invariant covariance Σ_i . In cases of static obstacles, $\mu_{ti} = \mu_i$. Note that this formulation applies to both single- and multi-aircraft systems.

Definition 1 (Collision Condition) A collision event occurs when the eVTOL is too close to an obstacle i, i.e.,

$$\|\boldsymbol{x}_t - \boldsymbol{c}_{ti}\| \le r_* + r_i \tag{4}$$

where x_t and c_{ti} are the locations of the current eVTOL and the obstacle i at time t, respectively. r_* and r_i are their safety ranges, respectively. Note that both x_t and c_{ti} are random variables, and therefore eq. (4) corresponds to an event, denoted by *collision*, in the probability space.

Given the collision condition defined above, this paper aims to find probabilistically guaranteed collision-free paths for a set of eVTOLs to reach their target locations, such that the probability of collision with any obstacle i at any time t is less than a certain threshold, i.e.,

$$\Pr(\text{collision}) \le \alpha$$
 (5)

where α is a prescribed threshold, called risk level.

3. RISK DOMAIN FORMULATION

In this section, we aim to bound the probability of an eVTOL avoiding collision with static or dynamic obstacles in the presence of both vehicle and obstacle uncertainty. Firstly, we study a simple case where the safety range of the current eVTOL and obstacle is negligible. In this case, we transform the possible region \mathcal{X}_{ti} in eq. (3) into a risk domain \mathcal{D}_{ti} at a given risk level α (or a confidence level $1 - \alpha$), which is proved to be a circle or an ellipse. Based on this, we further discuss the general case where the safety range is non-negligible. Finally, we introduce the concept of relative uncertainty to reduce both vehicle and obstacle uncertainty into a common form of uncertainty to simplify the process of feasibility checking for the probabilistic bounds.

3.1. Risk Domain Formulation for a Single Uncertain Obstacle

In this subsection, we consider a single obstacle whose location is subject to Gaussian distribution, and formulate the risk domain at a given risk level α for the obstacle that the

eVTOL seeks to evade. The location, x_t , of the eVTOL is assumed to be deterministic and the safety ranges for both the obstacle and the eVTOL are assumed to be infinitesimal, i.e. $r_i = r_* := \delta \to 0$. For the general cases of multiple obstacles and non-negligible safety ranges, we will discuss in Section 3.2 and section 3.3.

We first find the risk domain of a d-dimensional Gaussian random variable in Lemma 1. **Definition 2** (Risk Domain) A set $\mathcal{D} \subset \mathbb{R}^d$ that satisfies

$$\Pr(\boldsymbol{X} \in \mathcal{D}) \ge 1 - \alpha \tag{6}$$

is called the risk domain at risk level α of a random variable X.

Lemma 1 Let $X \in \mathbb{R}^d$ be a d-dimensional random variable that obeys a d-dimensional Gaussian distribution $\mathcal{N}_d(\boldsymbol{\mu}, \boldsymbol{\Sigma})$, then the following set

$$\mathcal{D} := \{ \boldsymbol{X} \mid (\boldsymbol{X} - \boldsymbol{\mu})^{\mathrm{T}} \boldsymbol{\Sigma}^{-1} (\boldsymbol{X} - \boldsymbol{\mu}) \le F_d^{-1} (1 - \alpha) \}$$
 (7)

specifies the risk domain of X at risk level α , where F_d^{-1} is the inverse mapping of the cumulative distribution function (CDF) of the chi-squared distribution with d degrees of freedom.

Proof: Since $X \sim \mathcal{N}_d(\mu, \Sigma)$, the probability density function (PDF) of X takes the following form [32]

$$f(\mathbf{X}) = \frac{1}{(2\pi)^{\frac{d}{2}} |\mathbf{\Sigma}|^{\frac{1}{2}}} \exp\left[-\frac{1}{2} (\mathbf{X} - \boldsymbol{\mu})^{\mathrm{T}} \mathbf{\Sigma}^{-1} (\mathbf{X} - \boldsymbol{\mu})\right]$$
(8)

where $\boldsymbol{\mu} \in \mathbb{R}^d$ and $\boldsymbol{\Sigma} \in \mathbb{R}^{d \times d}$ are the mean and covariance matrix of \boldsymbol{X} , respectively.

According to the theorem of quadratic distribution [33], it follows that a new quadratic random variable derived from X must obey a one-dimensional chi-squared distribution

$$Q = (\boldsymbol{X} - \boldsymbol{\mu})^{\mathrm{T}} \boldsymbol{\Sigma}^{-1} (\boldsymbol{X} - \boldsymbol{\mu}) \sim \chi_d^2, \tag{9}$$

where Q represents the one-dimensional quadratic random variable and χ_d^2 represents the one-dimensional chi-squared distribution with d degrees of freedom.

The CDF of Q is then given by [32]

$$F_d(q) = \Pr(Q \le q) = P\left(\frac{d}{2}, \frac{q}{2}\right) := p \tag{10}$$

where $P\left(\frac{d}{2}, \frac{q}{2}\right)$ is the regularized gamma function.

As $F_d(q): R^+ \to [0,1)$ is a bijective mapping, we can find the following inverse mapping for $F_d(q)$

$$q = F_d^{-1}(p) : [0, 1) \to R^+$$
 (11)

Given a risk level α (or confidence level $1-\alpha$), we have $p=1-\alpha$, then we can find a value $q_{1-\alpha}=F_d^{-1}(1-\alpha)$ such that

$$\Pr\left(Q \le q_{1-\alpha}\right) = \Pr\left(Q \le F_d^{-1}(1-\alpha)\right) = 1 - \alpha \tag{12}$$

According to eq. (9), it follows that the set

$$\{ \boldsymbol{X} \mid (\boldsymbol{X} - \boldsymbol{\mu})^{\mathrm{T}} \boldsymbol{\Sigma}^{-1} (\boldsymbol{X} - \boldsymbol{\mu}) \le q_{1-\alpha} = F_d^{-1} (1 - \alpha) \}$$
(13)

forms the risk domain \mathcal{D} of the random variable X at risk level α .

With Lemma 1, we can now formulate the risk domain at a given risk level α for the obstacle that the eVTOL seeks to evade. In particular, by restricting our attention to eVTOLs moving at the same altitude, i.e., d=2, we can find the risk domain \mathcal{D}_{ti} for obstacle i whose location $\mathbf{c}_{ti} \sim \mathcal{N}(\boldsymbol{\mu}_{ti}, \boldsymbol{\Sigma}_i)$ at time t, according to Lemma 1. Specifically,

$$\mathcal{D}_{ti} := \{ \boldsymbol{c}_{ti} \mid (\boldsymbol{c}_{ti} - \boldsymbol{\mu}_{ti})^{\mathrm{T}} \boldsymbol{\Sigma}_{i}^{-1} (\boldsymbol{c}_{ti} - \boldsymbol{\mu}_{ti}) \leq F_{2}^{-1} (1 - \alpha) \}$$
(14)

where

$$F_2^{-1}(1-\alpha) = -2\ln(\alpha) \tag{15}$$

as

$$F_2(q) = 1 - e^{-\frac{q}{2}} \tag{16}$$

Of note, the boundary of the risk domain \mathcal{D}_{ti} can be geometrically interpreted as a circle or an ellipse, depending on the values of the covariance Σ_i .

To ensure that the probability of collision is less than a particular risk level α , the eVTOL's location \boldsymbol{x}_t should be outside the corresponding risk domain \mathcal{D}_{ti} of obstacle i at time t, i.e.,

$$\left(\boldsymbol{x}_{t} - \boldsymbol{\mu}_{ti}\right)^{\mathrm{T}} \boldsymbol{\Sigma}_{i}^{-1} \left(\boldsymbol{x}_{t} - \boldsymbol{\mu}_{ti}\right) > F_{2}^{-1} (1 - \alpha), \tag{17}$$

as

Pr(collision | eq. (17) holds)
= Pr(
$$||\boldsymbol{c}_{ti} - \boldsymbol{x}_t|| \le r_* + r_i = 2\delta \mid \boldsymbol{x}_t \notin \mathcal{D}_{ti}$$
)
 $\le \Pr(\boldsymbol{c}_{ti} \notin \mathcal{D}_{ti})$
= Pr($(\boldsymbol{c}_{ti} - \boldsymbol{\mu}_{ti})^{\mathrm{T}} \boldsymbol{\Sigma}_i^{-1} (\boldsymbol{c}_{ti} - \boldsymbol{\mu}_{ti}) > F_2^{-1} (1 - \alpha)$)
= Pr($Q > q_{1-\alpha}$)
= α (18)

In the above inequality, $\Pr(||\boldsymbol{c}_{ti} - \boldsymbol{x}_t|| \leq 2\delta \mid \boldsymbol{x}_t \notin \mathcal{D}_{ti}) \leq \Pr(\boldsymbol{c}_{ti} \notin \mathcal{D}_{ti})$ holds because $\delta \to 0$, and then the obstacle needs to be outside of its corresponding risk domain \mathcal{D}_{ti} to meet the collision condition.

Note that the constraint in eq. (17) is a deterministic quadratic inequality that is tractable and can be easily implemented, compared with the probabilistic constraint in eq. (18). Moreover, the above discussion can be easily extended to higher dimension problems, such as d=3.

3.2. Risk Domain Formulation for Multiple Uncertain Obstacles

In this subsection, we consider a more general case where multiple uncertain obstacles (either static or dynamic) are present. The safety ranges for both obstacles and the eVTOL are still thought to be negligible.

To ensure the probability of collision with all the obstacles doesn't exceed a given threshold ϑ , we apply the same idea presented in the previous subsection. In particular, suppose there are N eVTOLs and environmental obstacles in total, with the location of each obstacle c_{ti} following a two-dimensional Gaussian distribution, i.e., $c_{ti} \sim \mathcal{N}_2(\boldsymbol{\mu}_{ti}, \boldsymbol{\Sigma}_i)$. According to the analysis in the previous subsection, the risk domain \mathcal{D}_{ti} of an obstacle i can be captured by eq. (14), where $\alpha = \vartheta/(N-1)$, and probabilistically guaranteed collision avoidance with this obstacle can be ensured by enforcing the deterministic constraint in eq. (17).

To ensure that the probability of collision with any of the obstacles is less than the threshold ϑ , the current eVTOL should avoid the risk domains formed by all the obstacles at each time step t. This can be achieved by introducing the following constraint

$$(\boldsymbol{x}_{t} - \boldsymbol{\mu}_{ti})^{\mathrm{T}} \boldsymbol{\Sigma}_{i}^{-1} (\boldsymbol{x}_{t} - \boldsymbol{\mu}_{ti}) > F_{2}^{-1} (1 - \alpha), \ \forall i \in \{1, \dots, N - 1\}$$
 (19)

as

Pr(collision | eq. (19) holds)

$$= \Pr(||\boldsymbol{c}_{ti} - \boldsymbol{x}_{t}|| \leq r_{*} + r_{i} = 2\delta, \ \forall i \in \{1, \dots, N-1\} | \ \boldsymbol{x}_{t} \notin \bigcup_{i=1}^{N-1} \mathcal{D}_{ti})$$

$$\leq \Pr(\bigvee_{i=1}^{N-1} (\boldsymbol{c}_{ti} - \boldsymbol{\mu}_{ti})^{\mathrm{T}} \boldsymbol{\Sigma}_{i}^{-1} (\boldsymbol{c}_{ti} - \boldsymbol{\mu}_{ti}) > F_{2}^{-1} (1 - \alpha))$$

$$\leq \sum_{i=1}^{N-1} \Pr((\boldsymbol{c}_{ti} - \boldsymbol{\mu}_{ti})^{\mathrm{T}} \boldsymbol{\Sigma}_{i}^{-1} (\boldsymbol{c}_{ti} - \boldsymbol{\mu}_{ti}) > F_{2}^{-1} (1 - \alpha))$$

$$\leq (N-1)\alpha = \vartheta$$

$$(20)$$

3.3. Risk Domain Formulation with Safety Range

In this subsection, we consider the even more general case where the safety range of the obstacle/eVTOL is non-negligible. For simplicity, the geometric shape of the safety range is assumed to be a time-invariant circle.

As shown in Fig. 1, the radius of the safety ranges for the obstacle and the eVTOL are r_i and r_* , respectively. The possible region \mathcal{X}_{ti} (as defined in eq. (3)) of the obstacle i at time t can be represented by the union of a series of circles with radius r_i , where the circle's center \mathbf{c}_{ti} , i.e. the location of the obstacle i, follows a Gaussian distribution. As discussed in Section 3.1, we can find the risk domain \mathcal{D}_{ti} for the obstacle i at time t, according to Lemma 1.

Furthermore, when considering the safety range r_i of obstacle i, the actual risk domain for obstacle i at time step t is indeed the enveloping area of a series of circles whose centers are inside or on the boundary of the risk domain \mathcal{D}_{ti} . We denote this actual domain as \mathcal{D}_{ti}^{range} , which is a larger area than \mathcal{D}_{ti} , as shown in Fig. 1.

Since there is no explicit expression of the actual risk domain \mathcal{D}_{ti}^{range} , we will check the feasibility of the constraints by measuring the minimum distance between the eVTOL's location \boldsymbol{x}_t and the risk domain of \boldsymbol{c}_{ti} , which is denoted as d_{\min} . In fact, d_{\min} can be treated as the distance from a point to an ellipse, which can be calculated explicitly according to [34]. Then we check the feasibility of the constraints using the inequality

$$d_{\min}(\boldsymbol{x}_t, \mathcal{D}_{ti}) > r_i + r_* \tag{21}$$

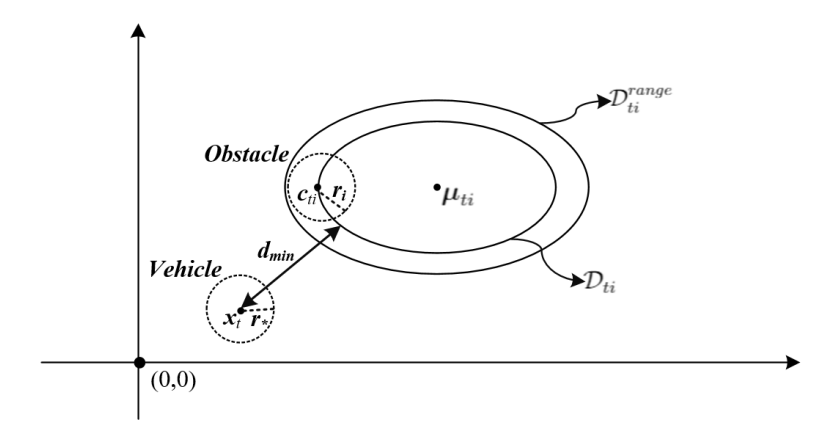


Figure 1: Schematic of the Safety Range

if it holds, then

Pr(collision | eq. (21) holds)
= Pr(
$$\|\boldsymbol{x}_{t} - \boldsymbol{c}_{ti}\| \leq r_{i} + r_{j} | \boldsymbol{x}_{t} \notin \mathcal{D}_{ti}^{range}$$
)
 $\leq Pr(\boldsymbol{c}_{ti} \notin \mathcal{D}_{ti})$
= α (22)

Thus, given a risk level α which denotes the probabilistic bound on the chance that the eVTOL collides with any obstacle i at any time step t, we can transform the probabilistic constraint eq. (22) into a deterministic constraint eq. (21) equivalently, in consideration of the safety ranges of both obstacles and eVTOLs.

3.4. Transformation of Relative Uncertainty

So far we have only considered the scenario where obstacle uncertainty exists. In this subsection, we consider both vehicle and obstacle uncertainty, and introduce the transformation of relative uncertainty, which can reduce both vehicle and obstacle uncertainty into one common uncertainty. With this, the risk domain formulation established above can then be smoothly extended to scenarios where both forms of uncertainty exist.

For the simplicity of notation, let random variable $\mathbf{X} = (x_1, x_2)^{\mathrm{T}}$ denote the location \mathbf{c}_{ti} of an obstacle i and random variable $\mathbf{Y} = (y_1, y_2)^{\mathrm{T}}$ denote the location \mathbf{x}_t of the current eVTOL at time step t. Thus, under the assumption of Gaussian distribution, it follows that

$$\boldsymbol{X} \sim \mathcal{N}\left((\mu_1, \mu_2)^{\mathrm{T}}, \begin{bmatrix} \sigma_{11} & \sigma_{12} \\ \sigma_{21} & \sigma_{22} \end{bmatrix}\right)$$

$$\boldsymbol{Y} \sim \mathcal{N}\left((v_1, v_2)^{\mathrm{T}}, \begin{bmatrix} \tau_{11} & \tau_{12} \\ \tau_{21} & \tau_{22} \end{bmatrix}\right)$$
(23)

Consider that both $Var(\boldsymbol{X})$ and $Var(\boldsymbol{Y})$ are expressed in a common coordinate system. It follows that the relative random variable $\boldsymbol{Z} = (\boldsymbol{X} - \boldsymbol{Y}) = (z_1, z_2)^T = (x_1 - y_1, x_2 - y_2)^T$ denotes the relative position with uncertainty between the obstacle i and the current eVTOL. It obeys a new Gaussian distribution [35], which is displayed as

$$Z \sim \mathcal{N}(\boldsymbol{\mu}, \boldsymbol{\Sigma})$$

 $\sim \mathcal{N}(E(\boldsymbol{X} - \boldsymbol{Y}), Var(\boldsymbol{X} - \boldsymbol{Y}))$ (24)

where the mean and covariance of Z are respectively represented by

$$\mu = \mathrm{E}(\boldsymbol{X} - \boldsymbol{Y})$$

$$= \mathrm{E}(\boldsymbol{X}) - \mathrm{E}(\boldsymbol{Y})$$

$$= (\mu_1 - v_1, \mu_2 - v_2)^{\mathrm{T}}$$

$$\boldsymbol{\Sigma} = \mathrm{Var}(\boldsymbol{X} - \boldsymbol{Y})$$

$$= \begin{bmatrix} \mathrm{Var}(z_1) & \mathrm{cov}(z_1, z_2) \\ \mathrm{cov}(z_1, z_2) & \mathrm{Var}(z_2) \end{bmatrix}$$

$$= \begin{bmatrix} \mathrm{Var}(x_1) + \mathrm{Var}(y_1) & \mathrm{cov}(z_1, z_2) \\ \mathrm{cov}(z_1, z_2) & \mathrm{Var}(x_2) + \mathrm{Var}(y_2) \end{bmatrix}$$

$$= \begin{bmatrix} \sigma_{11} + \tau_{11} & \rho \sqrt{\mathrm{Var}(z_1) \, \mathrm{Var}(z_2)} \\ \rho \sqrt{\mathrm{Var}(z_1) \, \mathrm{Var}(z_2)} & \sigma_{22} + \tau_{22} \end{bmatrix}$$
(25)

and ρ represents the correlation coefficient between the first and second component of \mathbf{Z} . For simplicity, we assume $\rho = 0$ in this paper and the covariance of \mathbf{Z} can be simplified as

$$\Sigma = Var(\boldsymbol{X} - \boldsymbol{Y})$$

$$= Var(\boldsymbol{X}) + Var(\boldsymbol{Y})$$
(26)

As a comparison to the aforementioned scenarios where both variances are expressed in a common coordinate system, it is more often to see that Var(X) is expressed in the body-fixed coordinate system of the obstacle i, whereas Var(Y) is also expressed in its own body-fixed coordinate system of the eVTOL. Therefore, it's necessary to perform coordinate transformations before the further transformations of relative uncertainty.

For reference, a ground coordinate system is first established. Relative to the ground coordinate system, we can find the orientation vectors $(\cos \alpha, \sin \alpha)^{\mathrm{T}}$ of the obstacle i and $(\cos \beta, \sin \beta)^{\mathrm{T}}$ of the eVTOL at the same time t. Note that now both variances, $\mathrm{Var}(\boldsymbol{X})$ and $\mathrm{Var}(\boldsymbol{Y})$, are expressed in their own body-fixed coordinate systems and can be re-expressed in the common ground coordinate system as follows

$$Var(\boldsymbol{X})' = \boldsymbol{J}_{obs} Var(\boldsymbol{X}) \boldsymbol{J}_{obs}^{T}$$

$$Var(\boldsymbol{Y})' = \boldsymbol{J}_{veh} Var(\boldsymbol{Y}) \boldsymbol{J}_{veh}^{T}$$
(27)

where

$$\mathbf{J}_{obs} = \begin{bmatrix} \cos \alpha & -\sin \alpha \\ \sin \alpha & \cos \alpha \end{bmatrix}
\mathbf{J}_{veh} = \begin{bmatrix} \cos \beta & -\sin \beta \\ \sin \beta & \cos \beta \end{bmatrix}$$
(28)

Therefore, the covariance of Z expressed in the ground coordinate system, denoted by Σ' , is displayed as

$$\Sigma' = \operatorname{Var}(\boldsymbol{X} - \boldsymbol{Y})'$$

$$= \operatorname{Var}(\boldsymbol{X})' + \operatorname{Var}(\boldsymbol{Y})'$$
(29)

For simplicity, the covariance of \boldsymbol{Z} can be further diagonalized through a coordinate transformation

$$\Sigma'' = U^{\mathrm{T}} \Sigma' U \tag{30}$$

where Σ'' is a diagonal matrix indicating the covariance of \mathbf{Z} , and \mathbf{U} is an orthogonal matrix whose every column vector is the corresponding eigenvector of the inverse matrix of Σ' . Also, the expected relative position $\boldsymbol{\mu}'' = (m, n)^{\mathrm{T}}$ between the obstacle i and the eVTOL takes the following form

$$\boldsymbol{\mu}'' = \boldsymbol{U}^{\mathrm{T}} (\mu_1 - v_1, \mu_2 - v_2)^{\mathrm{T}}$$
(31)

Through the transformation of relative uncertainty as well as coordinate transformation, the relationship between the location of obstacle X and eVTOL Y can be transformed to the relationship between Z and origin (0,0), as shown in Fig. 2. In other words, through the transformation, the original uncertain location of eVTOL Y (vehicle uncertainty) is transformed to a deterministic location (0,0) in the new relative coordination system, while its location uncertainty is added to the location uncertainty of the obstacle X.

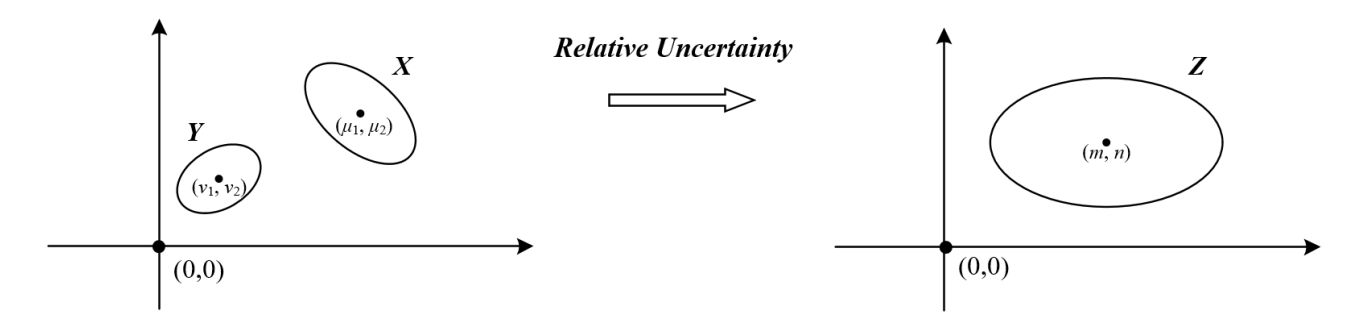


Figure 2: Schematic of the Transformation of Relative Uncertainty

According to the risk domain formulated in Section 3.3, we can also build the risk domain for the relative position Z between the *i*th obstacle and the eVTOL at time t

$$(Z - \mu'')^{\mathrm{T}} \Sigma''^{-1} (Z - \mu'') = F_2^{-1} (1 - \alpha)$$
 (32)

whose boundary is also a circle or an ellipse.

Similar to eq. (21), to check whether the eVTOL would collide with the obstacle, it's only required to check the minimum distance d_{\min} between the origin (0,0) and the elliptic risk domain eq. (32) whose center is $\boldsymbol{\mu}'' = (m, n)^{\mathrm{T}}$. If d_{\min} is greater than the safety range, the probability of collision will be bounded by the prescribed risk level α .

On the grounds of the discussion of relative uncertainty above, we successfully transform the vehicle and environmental obstacle uncertainties into one common uncertainty, instead of dealing with them separately.

4. RISK-BOUNDED AND FAIRNESS-AWARE PATH PLANNING

In this section, a risk-bounded and fairness-aware path planning algorithm based on the sampling-based method of tree search is developed. Through incorporating the risk domain formulation established in Section 3 and considering flight fairness, this proposed algorithm applies to not only a single eVTOL, but also a system consisting of multiple eVTOLs, in the presence of both vehicle and environmental obstacle uncertainties.

Based on the essentials of the sampling-based method of tree search, the proposed algorithm grows a tree to dynamically generate feasible trajectories, which satisfies the risk bound of collision probability at each node. It means that following the trajectory planned by the proposed path planning algorithm, the probability that the current eVTOL collides with obstacles doesn't exceed the prescribed risk level. The current eVTOL's location at each node is checked against the constraints with the nearby obstacles, by using the transformation of relative uncertainty described in Section 3.4. If the constraint doesn't hold, i.e., $d_{\min} < r_i + r*$, it means the probability of collision indeed exceeds the prescribed value and the current node should be discarded; otherwise, the current node should be reserved and may contribute to growing future paths.

We can use a directed graph G = (V, E) to represent the paths generated by the proposed risk-bounded and fairness-aware path planning algorithm. In that way, a feasible path can be interpreted as a vertex sequence $(\boldsymbol{v}_1, \boldsymbol{v}_2, \dots, \boldsymbol{v}_n)$, where $\boldsymbol{v}_1 = \boldsymbol{x}_{\text{start}}$ and $\boldsymbol{v}_n = \boldsymbol{x}_{\text{goal}}$. The edge $(\boldsymbol{v}_i, \boldsymbol{v}_{i+1}) \in E$ represents a path connecting two neighbouring nodes.

4.1. Risk-bounded Path Planning for Single-aircraft Systems under Uncertainty 4.1.1. Static Uncertain Obstacles

To begin with, consider a simple scenario where all the obstacles present are assumed to be static but uncertain. We utilize the risk domain formulation developed in Section 3, which applies a fixed probability bound $\vartheta/(N-1)$ across all the obstacles, leading to deterministic constraints that can be computed at each time step. With the risk domain formulation, one can determine whether the converted deterministic constraints are satisfied or not through evaluating the relative position between a sample point $\boldsymbol{x}_{\text{rand}}$ and the corresponding risk domain \mathcal{D}_i of obstacle i for all time steps at a given risk level α . The sample point $\boldsymbol{x}_{\text{rand}}$ is a node of the tree generated by risk-bounded path planning algorithm that doesn't violate the risk domain \mathcal{D}_i . It is guaranteed that each node of the tree satisfies the probability bound of collision with any obstacle i through the risk-bounded path planning.

The steps of the risk-bounded tree search (RTS) algorithm intended for such a scenario are presented in **Algorithm 1**.

4.1.2. Dynamic Uncertain Obstacles

Based on the risk-bounded path planning algorithm displayed in Algorithm 1, we proceed to consider a more complicated scenario where dynamic obstacles subject to Gaussian uncertainty are present. In particular, in this scenario, the risk domain \mathcal{D}_{ti} of each obstacle i varies over time. Such time dependence allows the inclusion of dynamic obstacles.

To address this scenario, we just need to figure out the risk domain \mathcal{D}_{ti} of each dynamic obstacle i at a particular time step t. The dynamic obstacle can then be viewed as a static obstacle at the same time step. By doing so, we can generalize what we conclude in Section 4.1.1 here. Specifically, we can determine whether equivalent deterministic constraints are satisfied or not by evaluating the relative position between a sample point x_{rand} and the corresponding risk domain \mathcal{D}_{ti} of obstacle i at this time step t. Moving forward to the next time step t+1, the same evaluation process can be performed again to check whether the probability of collision exceeds the prescribed risk bound. However, different from Section 4.1.1 where \mathcal{D}_i is constant for the static obstacle, here the risk domain \mathcal{D}_{ti} for the dynamic

Algorithm 1 RTS for Static Uncertain Obstacles

```
1: Vertex V \leftarrow \boldsymbol{x}_{\text{start}}, Edge E \leftarrow \emptyset, Iteration step k \leftarrow 0;
 2: Construct tree G by using V and E;
 3: while k < max
         Randomly pick a node \boldsymbol{x}_{\text{rand}};
 4:
         Find the node \boldsymbol{x}_{\text{nearest}} in the tree G nearest to \boldsymbol{x}_{\text{rand}};
 5:
 6:
         Generate a new node x_{\text{new}} outside tree G between x_{\text{nearest}} and x_{\text{rand}};
         Generate a new path p_{\text{new}} between x_{\text{nearest}} and x_{\text{new}};
 7:
 8:
         if NoIntersect(\boldsymbol{p}_{\text{new}}, \mathcal{D}_i)
              Add the new node \boldsymbol{x}_{\text{new}} to tree G;
 9:
10:
              Add the new path p_{\text{new}} to tree G;
11:
              if \|\boldsymbol{x}_{\text{new}} - \boldsymbol{x}_{\text{goal}}\| < \epsilon
12:
                   break;
13:
              end if
14:
         end if
         k \leftarrow k + 1;
15:
16: end while
```

obstacle is time-varying. Thus, \mathcal{D}_{ti} at the previous time step t should be updated by $\mathcal{D}_{(t+1)i}$ at the current time step t+1.

Another concern is that in most cases, the sequence number of a new node in the generated tree is inconsistent with the number of time steps, because a parent node in the tree may have more than one descendant node. To address this issue, we use the minimum number of steps m from the new node to the start point, rather than the sequence number, to correspond with the number of time steps.

The steps of the risk-bounded tree search (RTS) algorithm for dynamic uncertain obstacles are presented in **Algorithm 2**.

4.2. Risk-bounded Path Planning for Multi-aircraft Systems under Uncertainty

4.2.1. Fixed Order Path Planning

For the flying safety of a multi-aircraft system, in addition to environmental obstacles, the possibility of collision between any two eVTOLs also needs to be considered. This can be addressed by decomposing the problem into a set of single-aircraft path planning sub-problems, with each sub-problem solved in a pre-fixed iterative order by the algorithm of risk-bounded tree search.

Particularly, at the beginning of every new time step, when we are ready to extend the trajectory for the current eVTOL in the multi-aircraft system, the possible trajectories for any other eVTOLs within the same time step may have yet to be determined. In view of this, for the current eVTOL to be planned, the positions of other eVTOLs within the current time step are uncertain. Thus, when we perform the RTS algorithm given in Algorithm 2 to generate a new path for the current eVTOL in the system, all the other eVTOLs can be formulated as dynamic obstacles obeying Gaussian distribution. In fact, for conflict detection and avoidance for a team of eVTOLs, the risk domain formulation of the conflict between one pair of eVTOLs in the team is first considered. Then that formulation is

Algorithm 2 RTS for Dynamic Uncertain Obstacles

```
1: Vertex V \leftarrow \boldsymbol{x}_{\text{start}}, Edge E \leftarrow \emptyset, Iteration step k \leftarrow 0;
 2: Construct tree G by using V and E;
 3: while k < max
 4:
           Randomly pick a node x_{rand};
 5:
           Find the node x_{\text{nearest}} in the tree G nearest to x_{\text{rand}};
 6:
           Generate a new node x_{\text{new}} outside tree G between x_{\text{nearest}} and x_{\text{rand}};
          Generate a new path p_{\text{new}} between x_{\text{nearest}} and x_{\text{new}};
 7:
 8:
           Find minimum steps m from \boldsymbol{x}_{\text{nearest}} to \boldsymbol{x}_{\text{start}};
 9:
           Minimum steps from \boldsymbol{x}_{\text{new}} to \boldsymbol{x}_{\text{start}} m \leftarrow m + 1;
10:
           Find current time step t corresponding to m;
11:
           Find risk domain \mathcal{D}_{ti} of obstacle i at current time step t;
12:
           if NoIntersect(\boldsymbol{p}_{\text{new}}, \mathcal{D}_{ti})
                Add the new node \boldsymbol{x}_{\text{new}} to tree G;
13:
14:
                Add the new path \boldsymbol{p}_{\text{new}} to tree G;
15:
               \mathbf{if} \, \left\| \boldsymbol{x}_{\text{new}} - \boldsymbol{x}_{\text{goal}} \right\| < \epsilon
16:
                    break;
17:
               end if
18:
           end if
19:
           k \leftarrow k + 1;
20: end while
```

applied to every pair of eVTOLs in the team, so that we can ultimately perform inter-agent conflict checking between any two eVTOLs in the team. In doing so, the multi-aircraft path planning problem is reduced to a set of single-aircraft sub-problems. To further reduce the risk for one eVTOL to collide with the other eVTOLs in the team, we consider the uncertainties of eVTOLs at not only the current time step but also the next few steps ahead of time.

The steps of the RTS algorithm for multiple eVTOLs are summarized in **Algorithm 3**. Different eVTOLs perform RTS path planning in a fixed order. n represents the number of eVTOLs, and l represents the number of steps ahead of time. $\boldsymbol{x}_{i,k}$ is the location of eVTOL i at time step k. $\mathcal{T}_{i,k}$ is a set formed by the locations of eVTOL i at the current time step k and the next l steps. Π_k is a set formed by $\mathcal{T}_{i,k}$ for all the eVTOLs at the current time step k. $\mathcal{O}_{i,k}$ denotes the locations of all the other aircraft that the current aircraft i seeks to avoid in the course of l steps ahead of the current time step k.

4.2.2. Fairness-aware Path Planning

In Section 4.2.1, the strategy of fixed order path planning only ensures that the decisions taken by individual eVTOLs don't conflict. However, the rule of fixed order path planning ignores any substantial benefit from changing order for every eVTOL in the team, which could result in unnecessary delays. Alternatively, we present fairness-aware path planning in this subsection to address these issues. It relies on the distance between any individual eVTOL in the team and its respective goal position, and on the times of the eVTOL's delay caused by temporary stop. A score is introduced to reflect an eVTOL's motivation

Algorithm 3 RTS for Multiple eVTOLs

```
1: Start point x_{i,k}, x_{i,k+1}, \dots, x_{i,k+l} \ \forall i \in \{1, \dots, n\};
      \mathcal{T}_{i,k} = \{ m{x}_{i,k}, m{x}_{i,k+1}, \dots, m{x}_{i,k+l} \};
      Initial time step k \leftarrow 0;
  2: while k < max
  3:
           for i = 1 : n
  4:
               \Pi_k = \{\mathcal{T}_{1,k}, \mathcal{T}_{2,k}, \dots, \mathcal{T}_{i,k}, \dots, \mathcal{T}_{n,k}\};
               \mathcal{O}_{i,k} = \Pi_k - \{\mathcal{T}_{i,k}\};
  5:
               \mathcal{T}_{i,k} = RTS(\mathcal{O}_{i,k});
  6:
  7:
           end for
           if \|\boldsymbol{x}_{i,k} - \boldsymbol{x}_{\text{goal}}\| < \epsilon
  8:
  9:
               break;
10:
           end if
11:
            k \leftarrow k + 1;
12: end while
```

to change its order rather than cycling through eVTOLs in the fixed order. Specifically, the motivation of an eVTOL i to change its order can be quantitatively captured by the following motivation score,

$$Score := \frac{d(s_i, g_i) - d(\boldsymbol{x}_{i,k}, g_i)}{d(s_i, g_i)} + \beta \frac{n_i}{k}$$
(33)

The motivation score is composed of two terms. The first term is the ratio of the distance $d(\mathbf{x}_{i,k}, g_i)$ between the eVTOL's location and its goal position to the distance $d(s_i, g_i)$ between the eVTOL's start position and goal position. The second term is the ratio of the times of delay n_i caused by temporary stop to the current time step k. β is a weighting parameter which seeks to achieve a balance between the two terms.

At each iteration, a permit is used to identify which eVTOL owns the priority to perform the RTS algorithm given in Algorithm 2. Every individual eVTOL evaluates its motivation in a bid to be the permit holder. When the current permit holder finishes RTS path planning, it passes the permit to the next eVTOL with the highest motivation score, and so on. This procedure generates updated order path planning. eVTOLs that may benefit most from changing order can do so sooner, without waiting for other eVTOLs which have little motivation to change order. Note that if an eVTOL updates its order, the respective constraints imposed on the other eVTOLs must also be updated accordingly.

Most often, the eVTOL that is closest to its goal will typically own the highest motivation score, allowing it to complete its task sooner and then can be arranged to receive a new task, which improves the efficiency in terms of resource allocation. Moreover, this strategy can reduce the computation intensity and air traffic density, since once an individual eVTOL achieves its goal, it can be removed from the team with no further path plannings needed. Therefore, the distance between the eVTOL's location and its goal position is added to the first term of the motivation score.

There is also a great chance that an eVTOL with low motivation score may fail to find a feasible path for the current time step (i.e., the number of iteration steps of computation

exceeds the maximum limitation). To address this concern, since the eVTOL is capable of hovering in one place, we can introduce temporary stop nodes along the eVTOL's path where it can stop temporarily during the current time step in a bid to yield to other eVTOLs in the team. This not only saves computational time but also lowers the risk of collision with other eVTOLs. However, the temporary stop during the current step can lead to the delay of the eVTOL, and the delay contributes to decreasing the motivation score of the eVTOL. The low motivation score in turn increases the delay of the eVTOL in the future. To make a compensation, the number of the eVTOL's delay caused by temporary stop is added to the second term of the motivation score. This strategy to assign a permit to the delayed aircraft to raise its priority helps improve the flight fairness between different aircraft.

The steps of the risk-bounded and fairness-aware tree search (RFTS) algorithm with the strategy of permit assignment are presented in **Algorithm 4**.

```
Algorithm 4 RFTS for Multiple eVTOLs
```

```
1: Current time step k;
 2: Evaluate the motivation score for all the eVTOLs;
 3: Pass permit to the eVTOL with highest motivation score;
 4: for i = 1 : n
 5:
      if the current eVTOL i holds permit
 6:
        if iteration < max
 7:
          Perform RTS to generate a new path for the current eVTOL i;
 8:
        else
 9:
          Temporary stop for the current eVTOL i;
10:
11:
        Pass permit to the next eVTOL with highest motivation score;
12:
      else
13:
        Swap the index of the current eVTOL i and the permit holder;
14:
        if iteration < max
15:
          Perform RTS to generate a new path for the permit holder;
16:
        else
17:
          Temporary stop for the permit holder;
18:
        end if
19:
        Pass permit to the next eVTOL with highest motivation score;
20:
      end if
21: end for
```

5. SIMULATION STUDY

In this section, several simulation cases are evaluated to verify the probabilistic feasibility of the proposed RTS/RFTS path planning algorithm for a single eVTOL or multiple eVTOLs. The proposed algorithms were implemented in Python3.8 and simulations were run on an Intel Core i7 1.90GHz laptop with 16GB of RAM.

5.1. Experimental Setup

All the locations of the obstacles (either static or dynamic) in this section are assumed to be uncertain and the safety ranges are assumed to be circles. The radius of the safety range is set to r=0.3 for the environmental obstacles and r=0.1 for the eVTOLs. The static obstacle is located at $\mathbf{X}_{\text{sobs}} = (x, y) \sim \mathcal{N}(\boldsymbol{\mu}_{\text{sobs}}, \boldsymbol{\Sigma}_{\text{sobs}})$ with $\boldsymbol{\mu}_{\text{sobs}} = (3, 3)$ and $\boldsymbol{\Sigma}_{\text{sobs}} = \begin{bmatrix} \frac{1}{6} & 0; & 0 & \frac{1}{24} \end{bmatrix}$. The dynamic obstacle is located at $\mathbf{X}_{\text{dobs}} = (x, y) \sim \mathcal{N}(\boldsymbol{\mu}_{\text{dobs}}, \boldsymbol{\Sigma}_{\text{dobs}})$ with $\boldsymbol{\Sigma}_{\text{dobs}} = \begin{bmatrix} \frac{1}{6} & 0; & 0 & \frac{1}{24} \end{bmatrix}$, while $\boldsymbol{\mu}_{\text{dobs}}$ is a time-varying parameter determined by its known trajectory for all time steps. For the simplicity of notation, we denote all the covariances here as $\boldsymbol{\Sigma}$. The location of an eVTOL is set to $\boldsymbol{X}_{\text{eVTOL}} = (x, y) \sim \mathcal{N}(\boldsymbol{\mu}_{\text{eVTOL}}, \boldsymbol{\Sigma}_{\text{eVTOL}})$ with $\boldsymbol{\Sigma}_{\text{eVTOL}} = \begin{bmatrix} \frac{1}{24} & 0; & 0 & \frac{1}{96} \end{bmatrix}$, while $\boldsymbol{\mu}_{\text{eVTOL}}$ is time-varying and determined by the nodes of path generated by the proposed RTS/RFTS algorithm at each time step t. We compare the performance of our proposed RTS/RFTS algorithm with the traditional RRT algorithm which doesn't incorporate chance constraints formulation and Zhu et al.'s approximation method which linearizes the collision conditions to obtain linear chance constraints [18].

For a given risk level α in each case, the simulation is divided into two stages:

1. Stage I: RTS/RFTS Path Planning

- Formulate risk domain for every obstacle i at every time step t at the given risk level α .
- Run RTS/RFTS algorithm to find a path with the desired probabilistic feasibility for each eVTOL in the system.

2. Stage II: Validation with Random Trials

- Given a planned path, generate random points from the associated distribution, which represent the realization of each obstacle *i* and eVTOL at every time step *t*.
- Check whether the planned path under the given risk level α for each eVTOL given in stage I collides with each realized obstacle i whose location is generated randomly at every time step t.
- Perform random trials for 100 times for each risk level α under the current case. Count the number of collision occurrences.

5.2. Case 1: Static Uncertain Obstacle + Single Deterministic eVTOL

In this case, a static uncertain obstacle and a single deterministic eVTOL are considered. Figs. 3a-3c demonstrate sample paths generated by our proposed RTS at $\alpha = 0.20$, $\alpha = 0.10$, and $\alpha = 0.05$ respectively under the same covariance Σ . The red line indicates the planned path, the blue circle or ellipse indicates the risk domain of the static obstacle, and the yellow circle indicates the realized position of the static obstacle with safety range in a random trial. As shown in Tab. 1, the path planned by our proposed RTS can ensure that the probability of collision with the static obstacle at any time step t does not exceed the risk level α .

Tab. 2 compares the performances of different planning algorithms with different levels of covariances under the same risk level $\alpha = 0.05$. It illustrates that compared with the

Table 1: Efficiency and Safety of RTS under Different Risk Levels

Case #	Algorithm	$ \alpha $	Avg. Length	Avg. Chance of Collision
		0.20	18.1	7%
Case 1	RTS	0.10	18.6	4%
		0.05	20.9	3%
		0.20	18.4	5%
Case 2	RTS	0.10	20.3	2%
		0.05	21.7	1%
		0.20	21.4	6%
Case 3	RTS	0.10	24.8	3%
		0.05	26.2	2%

Table 2: Efficiency and Safety of Planning Algorithms under Different Covariance Levels (L: Avg. trajectory length; CC: Avg. chance of collision; CT: Avg. computational time in ms)

Cogo #	Algorithm	$1/4\Sigma$		Σ		4Σ				
Case #		L	$\overline{\mathbf{CC}}$	CT	L	$\overline{\text{CC}}$	\mathbf{CT}	L	$\overline{\text{CC}}$	$\overline{\mathrm{CT}}$
Case 1	RTS	19.2	3%	16.6	20.9	3%	18.8	22.1	4%	22.4
	Approximation	21.7	2%	17.0	22.9	3%	19.2	25.3	3%	23.5
	RRT	15.4	52%	15.2	16.3	57%	15.2	20.5	65%	15.2
Case 2	RTS	19.5	1%	19.3	21.7	1%	22.5	24.2	3%	26.7
	Approximation	22.0	1%	20.5	23.8	1%	24.0	26.5	2%	27.9
	RRT	16.3	51%	18.2	17.2	53%	18.2	21.4	62%	18.2
Case 3	RTS	23.5	1%	341.1	26.2	2%	385.6	29.1	3%	457.1
	Approximation	26.4	1%	359.8	28.5	1%	435.2	30.6	2%	548.9
	RRT	20.7	51%	311.2	21.6	55%	311.2	25.9	68%	311.2

traditional RRT which doesn't consider chance constraints, our proposed RTS algorithm and Zhu et al.'s approximation method both effectively identify probabilistically feasible paths for the eVTOL in the presence of a static and uncertain obstacle. Thanks to the more accurate bound offered by our proposed risk domain formulation than Zhu et al.'s approximation method, the RTS algorithm achieves the same level of safety guarantee with a shorter trajectory. The efficiency of our algorithm becomes more significant as the covariance increases.

5.3. Case 2: Static Uncertain Obstacle + Single Uncertain eVTOL

In this case, a static uncertain obstacle and a single uncertain eVTOL are considered. Figs. 4a-4c depict paths generated by our RTS algorithm at three risk levels $\alpha=0.20$, $\alpha=0.10$, and $\alpha=0.05$, respectively. Here, the red ellipse indicates the risk domain of the eVTOL due to its vehicle uncertainty, others are the same with Case 1. The transformation of relative uncertainty is applied to convert both risk domains of the eVTOL and the static obstacle into a common one. The simulation results under different risk levels with the same covariance Σ are summarized in Tab. 1, which illustrates that the proposed RTS can effectively identify a probabilistically feasible path for the eVTOL in the presence of

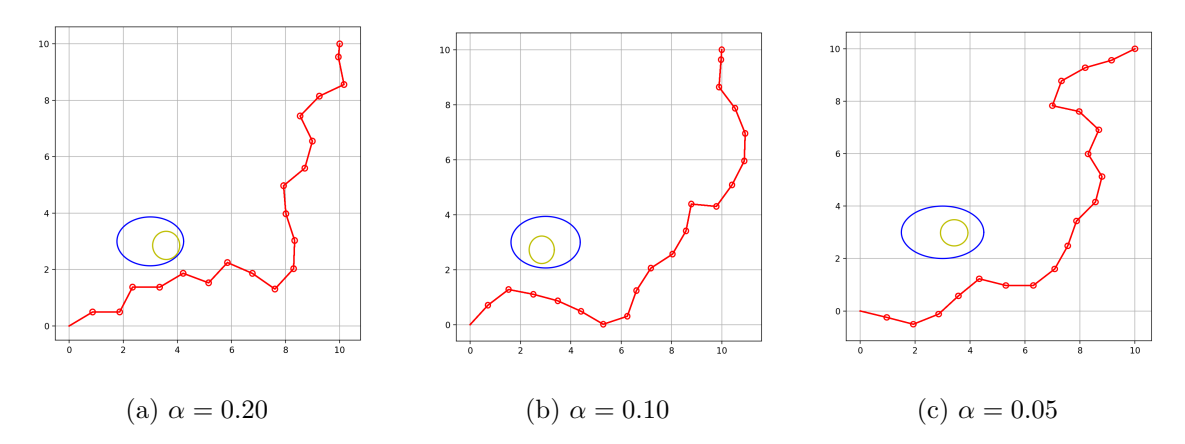


Figure 3: Case 1 RTS for Static Uncertain Obstacle + Single Deterministic eVTOL

both vehicle and static obstacle uncertainty. Similar to Case 1, Tab. 2 indicates that as compared to Zhu et al.'s approximation method and the traditional RRT algorithm at the same risk level $\alpha=0.05$, our algorithm generates shorter paths while satisfying the safety requirement.

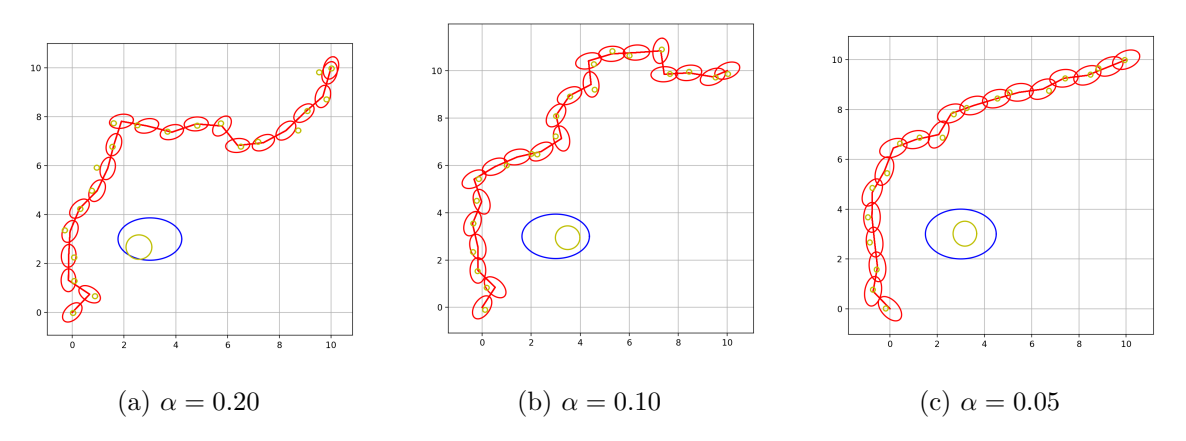


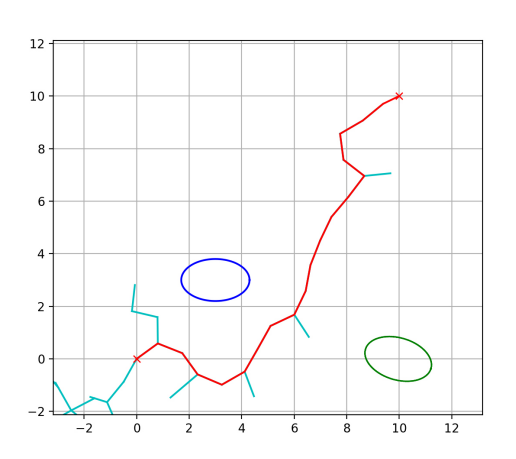
Figure 4: Case 2 RTS for Static Uncertain Obstacle + Single Uncertain eVTOL

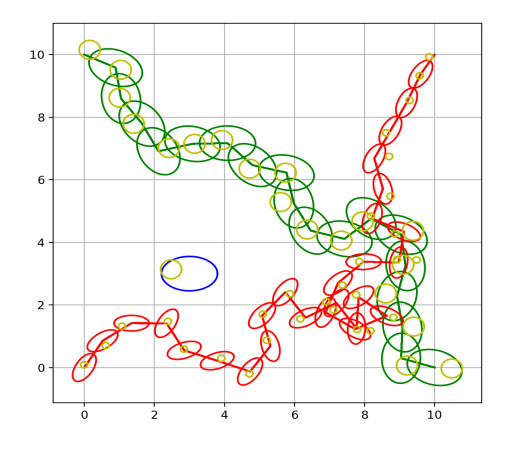
5.4. Case 3: Dynamic Uncertain Obstacle + Single Uncertain eVTOL

In this case, two obstacles are considered. One is static and the other one is dynamic. Both obstacles and the eVTOL are subject to Gaussian uncertainties.

Fig. 5a visualizes the procedure of RTS path planning at a particular time step when $\alpha=0.05$. The green ellipse which moves forward represents the risk domain of the dynamic obstacle while the blue one represents the risk domain of the static obstacle. The red line is the planned trajectory at the current time step and the light blue lines are the explored trajectories. In Fig. 5b, the red line indicates the final trajectory of the eVTOL planned by RTS, and the newly added green ellipse indicates the risk domain of the dynamic obstacle at all time steps. Moreover, the transformation of relative uncertainty is applied to convert risk

domains of both the eVTOL and the static/dynamic obstacle into a common one. Clearly, our proposed algorithm can also handle the dynamic obstacle in uncertain environments. Tab. 1 summarizes the simulation results under different risk levels with respect to the same covariance Σ . In general, a lower risk level produces more conservative solutions with a less collision chance and longer paths, which is well demonstrated in all the above three cases. The proposed RTS algorithm provides a quantitative bound to balance the risk and efficiency. Furthermore, Tab. 2 suggests that our algorithm achieves a good balance between the efficiency and safety.





- (a) planning process with red line as current planned trajectory and the blue lines as explored trajectories
- (b) result of RTS for an eVTOL

Figure 5: Case 3 RTS for Dynamic Uncertain Obstacle + Single Uncertain eVTOL

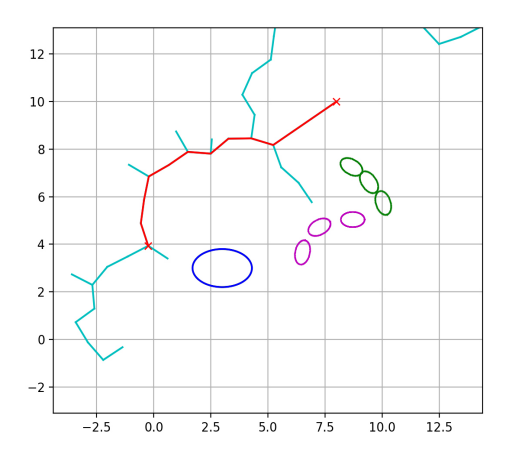
5.5. Case 4: RTS for Multiple Uncertain eVTOLs

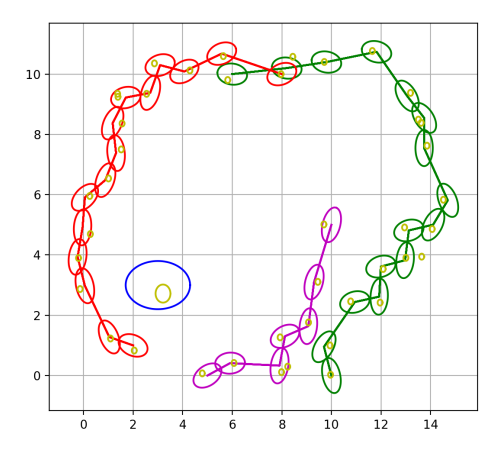
In this case, the risk-bounded path planning for a system consisting of three eVTOLs in the presence of a static obstacle is studied as a demo. The positions of both the eVTOLs and the static obstacle obey the pre-defined Gaussian distributions with time-varying means.

The risk-bounded path planning is carried out with the risk level set to $\alpha=0.05$. Different eVTOLs perform RTS path planning in a fixed order. As shown in Fig. 6a, when performing the RTS algorithm for an eVTOL, the other two eVTOLs are viewed as dynamic obstacles at the current time step, and their uncertainties at the current time step as well as the next two steps are considered based on their previous step's planning, shown as green and purple ellipses. Those three look-ahead steps help reduce the risk of collision in the future. In Fig. 6b, the red, purple, and green lines indicate the paths generated by the RTS algorithm for multiple eVTOLs in the team, respectively.

5.6. Case 5: RFTS for Multiple Uncertain eVTOLs

To improve the efficiency of multi-aircraft path planning with the risk-bounded path planning algorithm, the new feature of fairness-awareness is introduced in this case as a comparison to the strategy of fixed order path planning employed in Case 4, under the same





- (a) planning process with red line as current planned (b) result of RTS for multiple eVTOLs trajectory and the blue lines as explored trajectories

Figure 6: Case 4 RTS for Multiple Uncertain eVTOLs

risk level $\alpha = 0.05$ and the same covariance level Σ . The maximum iteration is set to 500. If the trajectory is identified within the maximum iteration steps, we deem it a feasible risk-bounded path. The values are only computed from successful runs.

Fig. 7a shows that according to the RFTS algorithm, the eVTOL (the red point) which is the permit holder, i.e., (10,5), will perform path planning earlier than the other eVTOLs in the team. Fig. 7b shows such a possibility that for an eVTOL (the red point) in the team, its possible way to the goal position may be blocked by the other eVTOLs (black ellipses) or the environmental obstacles, which makes it hard to find a feasible way (the red line). By applying the RFTS algorithm, such an eVTOL can stop for a while (one time step or more) to yield to the other eVTOLs since the eVTOL is capable of hovering in one place, which saves computational time. The delay of the eVTOL caused by the temporary stop increases its motivation score and therefore raises its flight priority in the future, which helps improve the flight fairness among different aircraft in the team.

Fig. 7c shows a scenario where an eVTOL has already reached its goal, and thus can be removed from the system (only black ellipses need to be considered), which eases the traffic density. The black, purple, and green line in Fig. 7d represent the paths generated by the RFTS algorithm for all three eVTOLs in the team at all time steps. Tab. 3 illustrates that compared with the fixed order path planning in Case 4, the RFTS algorithm can greatly reduce the length of the trajectory and increase the success rate of the path planning for the operation of multi-aircraft systems.

Table 3: Case 5 Efficiency and Safety of RTS and RFTS

Algorithm	Path Found	Avg. Length	Avg. Chance of Collision
RTS	5/10	37.5	$\frac{4\%}{2\%}$
RFTS	10/10	27.4	

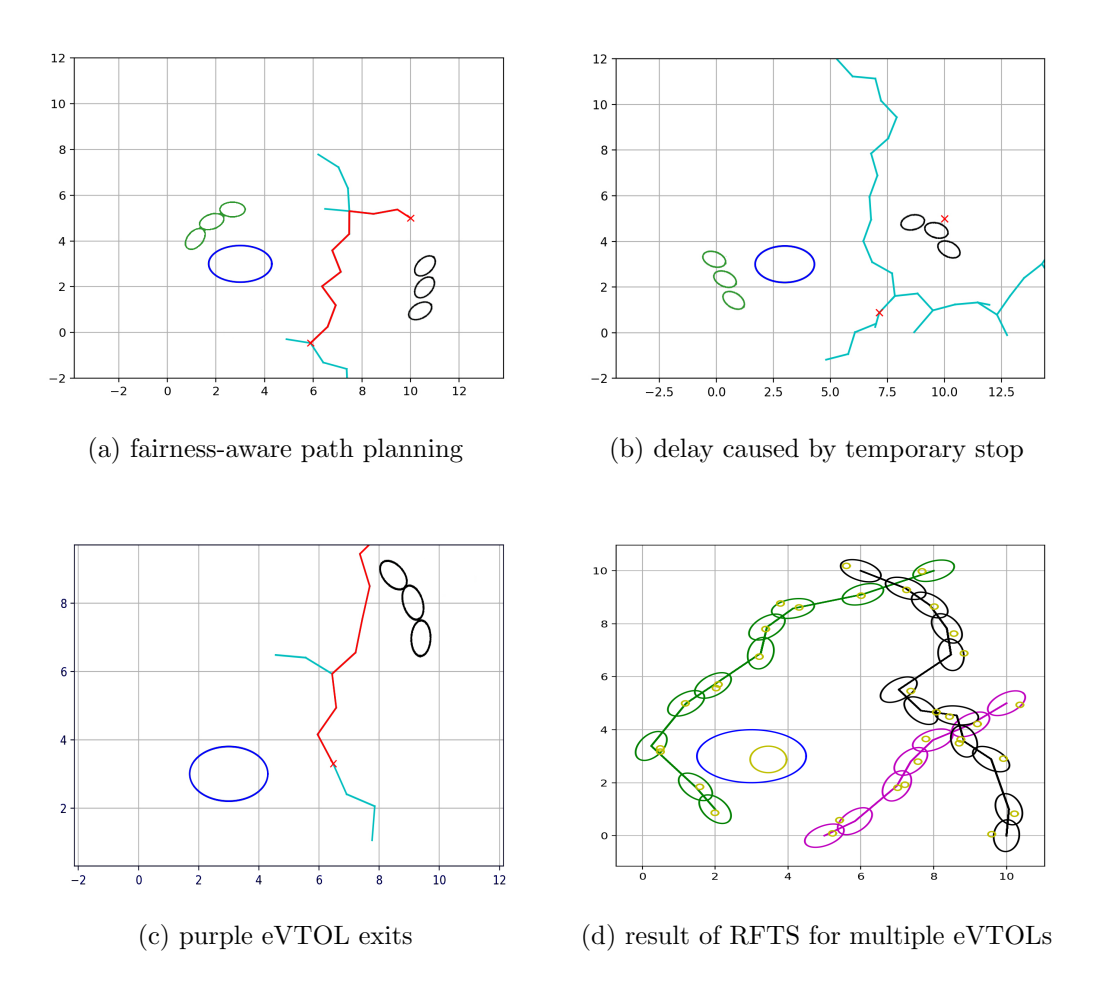


Figure 7: Case 5 RFTS for Multiple Uncertain eVTOLs

6. CONCLUSIONS

In this paper, a risk-bounded and fairness-aware algorithm based on the sampling-based method of tree search is presented for the path planning of a team of eVTOLs in the free flight airspace of UAM, which allows for either static or dynamic uncertain obstacles. By converting possible regions of obstacles into corresponding risk domains, the probabilistic constraints can be transformed into deterministic ones. Also, through the introduction of relative uncertainty, this approach can be applied to scenarios where both eVTOL and

environmental obstacle uncertainties exist. In addition, the strategy of permit assignment is designed to help improve flight fairness. Simulation results show that while considering flight fairness, the paths generated by the proposed path planning algorithm are probabilistically feasible in terms of avoiding collisions, and are shorter than the ones generated by the state-of-the-art algorithms.

In the future, we will consider scenarios where the communication network may fail. We are also working on scenarios where the location uncertainties obey non-Gaussian distributions by using non-parametric kernel density estimation.

ACKNOWLEDGMENTS

This work was supported by the National Science Foundation under Grants CMMI-2138612, CMMI-1944068, CNS-1953048, and CAREER-2048266.

References

- [1] D. P. Thipphavong, R. Apaza, B. Barmore, V. Battiste, B. Burian, Q. Dao, M. Feary, S. Go, K. H. Goodrich, J. Homola, et al., Urban air mobility airspace integration concepts and considerations, in: 2018 Aviation Technology, Integration, and Operations Conference, 2018, p. 3676.
- [2] S. Sawadsitang, D. Niyato, P.-S. Tan, P. Wang, Joint ground and aerial package delivery services: A stochastic optimization approach, IEEE Transactions on Intelligent Transportation Systems 20 (2018) 2241–2254.
- [3] A. Bauranov, J. Rakas, Designing airspace for urban air mobility: A review of concepts and approaches, Progress in Aerospace Sciences 125 (2021) 100726.
- [4] M. Wang, J. Diepolder, S. Zhang, M. Söpper, F. Holzapfel, Trajectory optimization-based maneuverability assessment of evtol aircraft, Aerospace Science and Technology 117 (2021) 106903.
- [5] M. D. Pavel, Understanding the control characteristics of electric vertical take-off and landing (evtol) aircraft for urban air mobility, Aerospace Science and Technology (2021) 107143.
- [6] X. Yang, P. Wei, Autonomous free flight operations in urban air mobility with computational guidance and collision avoidance, IEEE Transactions on Intelligent Transportation Systems (2021).
- [7] Y. Yang, J. Zhang, K.-Q. Cai, M. Prandini, Multi-aircraft conflict detection and resolution based on probabilistic reach sets, IEEE Transactions on Control Systems Technology 25 (2016) 309–316.
- [8] T. Lew, R. Bonalli, M. Pavone, Chance-constrained sequential convex programming for robust trajectory optimization, in: 2020 European Control Conference (ECC), IEEE, 2020, pp. 1871–1878.

- [9] S. Prentice, N. Roy, The belief roadmap: Efficient planning in linear pomdps by factoring the covariance, in: Robotics research, Springer, 2010, pp. 293–305.
- [10] R. Pepy, A. Lambert, Safe path planning in an uncertain-configuration space using rrt, in: 2006 IEEE/RSJ International Conference on Intelligent Robots and Systems, IEEE, 2006, pp. 5376–5381.
- [11] B. Luders, M. Kothari, J. How, Chance constrained rrt for probabilistic robustness to environmental uncertainty, in: AIAA guidance, navigation, and control conference, 2010, p. 8160.
- [12] P. Li, M. Wendt, G. Wozny, A probabilistically constrained model predictive controller, Automatica 38 (2002) 1171–1176.
- [13] J. Chen, l. Chen, D. Sun, Air traffic flow management under uncertainty using chance-constrained optimization, Transportation Research Part B: Methodological 102 (2017) 124–141.
- [14] L. Blackmore, M. Ono, A. Bektassov, B. C. Williams, A probabilistic particle-control approximation of chance-constrained stochastic predictive control, IEEE transactions on Robotics 26 (2010) 502–517.
- [15] L. Blackmore, M. Ono, B. C. Williams, Chance-constrained optimal path planning with obstacles, IEEE Transactions on Robotics 27 (2011) 1080–1094.
- [16] N. Du Toit, Robot motion planning in dynamic, cluttered, and uncertain environments: the Partially Closed-Loop Receding Horizon Control approach, Ph.D. thesis, California Institute of Technology, 2010.
- [17] M. Castillo-Lopez, P. Ludivig, S. A. Sajadi-Alamdari, J. L. Sanchez-Lopez, M. A. Olivares-Mendez, H. Voos, A real-time approach for chance-constrained motion planning with dynamic obstacles, IEEE Robotics and Automation Letters 5 (2020) 3620–3625.
- [18] H. Zhu, J. Alonso-Mora, Chance-constrained collision avoidance for mavs in dynamic environments, IEEE Robotics and Automation Letters 4 (2019) 776–783.
- [19] P. Scerri, S. Owens, B. Yu, K. Sycara, A decentralized approach to space deconfliction, in: 2007 10th international conference on information fusion, IEEE, 2007, pp. 1–8.
- [20] O. Purwin, R. D'Andrea, Path planning by negotiation for decentralized agents, in: 2007 American Control Conference, IEEE, 2007, pp. 5296–5301.
- [21] Y. Kuwata, A. Richards, T. Schouwenaars, J. P. How, Decentralized robust receding horizon control for multi-vehicle guidance, in: 2006 American Control Conference, IEEE, 2006, pp. 6–pp.
- [22] R. Vishnu, J. P. How, Decentralized path planning for multi-agent teams with complex constraints, Autonomous Robots 32 (2012) 385–403.

- [23] V. R. Desaraju, J. P. How, Decentralized path planning for multi-agent teams in complex environments using rapidly-exploring random trees, in: 2011 IEEE International Conference on Robotics and Automation, IEEE, 2011, pp. 4956–4961.
- [24] M. Radmanesh, M. Kumar, Flight formation of uavs in presence of moving obstacles using fast-dynamic mixed integer linear programming, Aerospace Science and Technology 50 (2016) 149–160.
- [25] A. U. Raghunathan, V. Gopal, D. Subramanian, L. T. Biegler, T. Samad, Dynamic optimization strategies for three-dimensional conflict resolution of multiple aircraft, Journal of guidance, control, and dynamics 27 (2004) 586–594.
- [26] Z. Wei, H. Wen, H. Hu, D. Jin, Ground experiment on rendezvous and docking with a spinning target using multistage control strategy, Aerospace Science and Technology 104 (2020) 105967.
- [27] Z. Zhao, H. Shang, Y. Dong, H. Wang, Multi-phase trajectory optimization of aerospace vehicle using sequential penalized convex relaxation, Aerospace Science and Technology 119 (2021) 107175.
- [28] G. S. Aoude, B. D. Luders, J. M. Joseph, N. Roy, J. P. How, Probabilistically safe motion planning to avoid dynamic obstacles with uncertain motion patterns, Autonomous Robots 35 (2013) 51–76.
- [29] S. M. LaValle, Rapidly-exploring random trees: A new tool for path planning (1998).
- [30] J. W. Woo, J.-Y. An, M. G. Cho, C.-J. Kim, Integration of path planning, trajectory generation and trajectory tracking control for aircraft mission autonomy, Aerospace Science and Technology 118 (2021) 107014.
- [31] Y. Liu, A progressive motion-planning algorithm and traffic flow analysis for high-density 2d traffic, Transportation Science 53 (2019) 1501–1525.
- [32] R. Vershynin, High-dimensional probability: An introduction with applications in data science, volume 47, Cambridge university press, 2018.
- [33] H. Hotelling, The generalization of student's ratio, in: Breakthroughs in statistics, Springer, 1992, pp. 54–65.
- [34] V. A. Zorich, Mathematical analysis II, Springer, 2016.
- [35] T. A. Snijders, Multilevel analysis, Springer, 2011.